



ACADEMIC  
PRESS

Available online at [www.sciencedirect.com](http://www.sciencedirect.com)

SCIENCE @ DIRECT®

Journal of Magnetic Resonance 158 (2002) 43–51

JMR

Journal of  
Magnetic Resonance

[www.academicpress.com](http://www.academicpress.com)

## Two dimensional prolate spheroidal wave functions for MRI

Qing X. Yang,<sup>a,\*</sup> Martin A. Lindquist,<sup>b</sup> Lawrence Shepp,<sup>b</sup> Cun-Hui Zhang,<sup>b</sup> Jianli Wang,<sup>a</sup>  
and Michael B. Smith<sup>a</sup>

<sup>a</sup> Department of Radiology (Center for NMR Research), The Pennsylvania State University, College of Medicine, The Milton S. Hershey Medical Center, 500 University Dr., Hershey, PA 17033, USA

<sup>b</sup> Department of Statistics, Rutgers University, New Brunswick, NJ 08854, USA

Received 22 January 2002; revised 15 July 2002

### Abstract

The tradeoff between spatial and temporal resolution is often used to increase data acquisition speed for dynamic MR imaging. Reduction of the  $k$ -space sampling area, however, leads to stronger partial volume and truncation effects. A two dimensional prolate spheroidal wave function (2D-PSWF) method is developed to address these problems. Utilizing prior knowledge of a given region of interest (ROI) and the spatial resolution requirement as constraints, this method tailors the  $k$ -space sampling area with a matching 2D-PSWF filter so that optimal signal concentration and minimal truncation artifacts are achieved. The  $k$ -space sampling area is reduced because the shape and size of the sampling area match the resolution posed by the non-rectangular shape of a convex ROI. The 2D-PSWF method offers an efficient way for spatial and temporal tradeoff with minimal penalty due to truncation, and thus, it promises a wide range of applications in MRI research.

© 2002 Elsevier Science (USA). All rights reserved.

**Keywords:** Magnetic resonance imaging; Signal processing;  $k$ -Space sampling; Prolate spheroidal wave function; Rapid data acquisition

### 1. Introduction

Many methods have been proposed to increase the temporal resolution for dynamic MR studies [1–9]. Because of the hardware limitations, and because the threshold of neuro-stimulation by rapidly switching gradients set an ultimate physical limit for imaging acquisition rate,  $k$ -space sampling must often be economized to meet the demands for image resolution, signal-to-noise ratio (SNR), and acquisition speed for a specific experiment. The keyhole technique exploits the fact that the central region of  $k$ -space contributes to the image intensity and contrast, while the peripheral regions contribute to image resolution details [1]. Since the dynamic variable in tissue perfusion and fMRI studies is the image intensity, while the geometry and the anatomic details of the image remain static, the keyhole technique can significantly improve the temporal resolution in

these studies by sampling only the central  $k$ -space area during dynamic data acquisition, and recycling the high spatial frequency area from a reference full  $k$ -space image [2]. Reducing the number of sampling points can also be achieved with singular value decomposition [3,4] and generalized series reconstruction [6] methods. In these methods, a priori information (a high-resolution reference image) is incorporated with the reduced-sampling data in order to maintain the spatial resolution of the dynamic images. Reduction of  $k$ -space sampling can also be achieved with multiple coil techniques such as SENSE [7] and SMASH [8]. With multiple coil techniques, the prior knowledge about RF field distributions, or image sensitivity of the coils, are utilized for image construction from under-sampled  $k$ -space data.

The trade-off between spatial and temporal resolution is often used to increase data sampling speed required by many applications [10–15]. Reducing image spatial resolution, however, leads to a stronger partial-volume effect, which decreases the sensitivity to dynamic signals such as BOLD contrast for detection of neuroactivities. The origin of the problem is the disparity between the

\* Corresponding author. Fax: 1-717-531-8486.  
E-mail address: [qyang@psu.edu](mailto:qyang@psu.edu) (Q.X. Yang).

size and irregular geometry of the region of interest (ROI), and the rectangular voxel produced by the fast Fourier transform [16]. In order to solve this problem, we present an alternative data acquisition and processing approach that tailors the  $k$ -space sampling area according to the size and shape of a convex ROI, and creates a matching two-dimensional prolate spheroidal wave function (2D-PSWF) filter [17–19] to optimally reduce truncation effect. With this new approach, the spatial information in reduced  $k$ -space data is used to calculate the total image intensity of non-square ROIs instead of a low-resolution image. In the 2D-PSWF method, a reference image is utilized as a priori to determine the features of the ROI. This method can be used for tracking dynamic signals from non-square ROIs with a reduced  $k$ -space sampling area with minimal signal leakage. It can also be applied to conventional square  $k$ -space as a post-processing method.

## 2. Theory

Consider a convex ROI,  $B$ , consisting of  $b$  pixels in image-space. Our objective is to determine the optimal sampling region,  $A$ , of a predetermined size  $a$ , which maximizes the total signal over the region  $B$  in image-space. We achieve this by designing a  $k$ -space sampling region based on the size and shape of given  $B$  with a matched two-dimensional filter that maximizes the energy concentration in  $B$ .

For an arbitrarily shaped  $B$  in image-space, consider a sub-region  $A$  of size  $a$  in  $k$ -space. We seek a function  $g(\mathbf{k})$  associated with  $A$  that satisfies the following two criteria:

1. It vanishes off  $A$ .
2. Its inverse Fourier transform,  $G(\mathbf{x})$ , has maximal signal concentration in  $B$ , i.e. the ratio

$$\frac{\int_B |G(\mathbf{x})|^2 d\mathbf{x}}{\int_\infty |G(\mathbf{x})|^2 d\mathbf{x}} \quad (1)$$

is maximized over all possible functions for which criterion (1) holds.

Now let  $A$  vary among all possible  $k$ -space regions of a given size  $a$ . For each possible region we will obtain a corresponding  $g(\mathbf{k})$  for which the above criteria hold. Then, choose the region whose corresponding  $g(\mathbf{k})$  makes the maximal concentration ratio in (2) as large as possible.

Let us assume that  $f(\mathbf{k})$  is the experimental sampling function in  $k$ -space and  $F(\mathbf{x})$  is its corresponding Fourier transform (the image). According to Parseval's identity, we have

$$\int_\infty F(\mathbf{x})G^*(\mathbf{x}) d\mathbf{x} = \int_\infty f(\mathbf{k})g^*(\mathbf{k}) d\mathbf{k}, \quad (2)$$

where “\*” represents the complex conjugate operation on a given function. The integral on the left-hand side of Eq. (2) is the image convolved with  $G(\mathbf{x})$ , a function that takes almost all its value inside of the ROI  $B$  and is essentially 0 outside of  $B$ . This integral is the weighted sum of the image over the ROI, which can be viewed as a reasonable proxy for the sum of the signal over  $B$ . A more stringent justification of this statement will come later in this section. For now let us assume that

$$\int_B F(\mathbf{x}) d\mathbf{x} \propto \int_\infty F(\mathbf{x})G^*(\mathbf{x}) d\mathbf{x} = \int_A f(\mathbf{k})g^*(\mathbf{k}) d\mathbf{k}. \quad (3)$$

As indicated above, the equation shows that the integral of the signal intensity over  $B$  can be approximated using a reduced area of  $k$ -space,  $\mathbf{k} \in A$ , since  $g(\mathbf{k}) = 0$  outside of  $A$ . Thus, if we are interested in obtaining the total signal intensity over a given ROI in an image, the sampling of  $k$ -space can be reduced to a region  $A$ . Using Eq. (3) the image intensity over the ROI  $B$  can be calculated directly from  $k$ -space area  $A$ .

Our problem consists of two parts:

- (I) Finding the sampling region  $A$ , of size  $a$ , which gives us the most information about a specific  $B$ .
- (II) Finding the optimal  $g(\mathbf{k})$ , which is determined by the choice of  $A$  and  $B$ .

These two parts are closely intertwined. To calculate  $g(\mathbf{k})$ , one needs the ROI  $B$  and the chosen sampling region  $A$  as input. The problem of finding  $g(\mathbf{k})$  is a 2D generalization of the theory of prolate spheroidal wave functions (PSWFs). The PSWF theory in one-dimension was developed by Slepian et al. [20–22]. A further review of PSWF theory can be found in Percival and Walden [23].

Finding the simultaneous solution for  $A$  and  $g(\mathbf{k})$  is a difficult mathematical problem. In theory, to find the optimal sampling region  $A$  we need to calculate the corresponding 2D-PSWF filters for all possible sampling schemes of a given size. It involves an exponential growth in  $N$  computer searches for an  $N \times N$  size image. To avoid such an extremely computer-intensive search we use a heuristic sampling scheme that has been proven by computer searches to be nearly optimal [17]. For the purpose of applying the 2D-PSWF theory to MRI data acquisition, the heuristic sampling region  $A$  and the corresponding optimal filter  $g(\mathbf{k})$  can be calculated as follows.

### 2.1. Determining $A$ , given $B$ (Heuristic solution)

The nature of the Fourier transform does not allow one to partially sample  $k$ -space and still obtain full information about a compact region in image-space. In one dimension, the problem of finding the optimal sampling region for a block of consecutive points in image-space was shown by Donoho and Stark [24] to consist of a block of consecutive points centered in the middle of  $k$ -space. If one chooses to sample a larger interval in  $k$ -space, then a finer interval of image-space

can be effectively resolved. Similarly, if one chooses to sample a shorter interval of  $k$ -space, one can only resolve coarser intervals in image-space. In the 2D case, this inverse relationship must be applied to all the orientations in the 2D plane to match the spatial frequency requirement by the shape and size of the ROI in image-space. Heuristically, this can be achieved by choosing  $A$  with a shape that is rotated in-plane  $90^\circ$  from  $B$ . The heuristic sampling region  $A$ , given a ROI  $B$ , can be determined as described below.

1. Center  $B$  so that its center of mass lies in the center of the image.
2. Define a region of  $k$ -space,  $H'$ , whose coordinates coincide with those of  $B$ .
3. Define an auxiliary region,  $H$ , obtained by rotating  $H'$   $90^\circ$ , i.e.

$$H = \{(-j, i) \mid (i, j) \in H'\}. \quad (4)$$

4. The shape of  $A$  is determined by taking the union of  $H$  and  $(-H)$  to assure that  $A$  has a symmetric shape.
5. The region  $A$  is scaled to size  $a$ .

The criteria for choosing the size of the sampling region  $a$  will be given later in this section.

## 2.2. Determining the optimal $g(\mathbf{k})$ , given $A$ , and $B$

For a given  $A$ ,  $g(\mathbf{k})$  is obtained by finding the function whose inverse Fourier transform maximizes Eq. (1). With proper normalization of  $G(\mathbf{x})$  we can assume that

$$\int_{-\infty}^{\infty} |G(\mathbf{x})|^2 d\mathbf{x} = 1. \quad (5)$$

The problem becomes finding the solution to the following equation,  $\lambda$ , subject to the above constraint on  $G(\mathbf{x})$ :

$$\lambda = \max \int_B |G(\mathbf{x})|^2 d\mathbf{x} = \max \sum_B G(\mathbf{x}) G^*(\mathbf{x}). \quad (6)$$

To simplify the calculation, we will write the Fourier transform in matrix form. Let  $\mathbf{T}$  be the  $N^d \times N^d$  discrete Fourier transform matrix with elements

$$\exp\{-i2\pi(\mathbf{x}, \mathbf{k})/N\}/N^{d/2}, \quad (7)$$

where  $d$  is the dimension of  $k$ -space. Let  $\mathbf{T}^{-1}$  denote the inverse Fourier transform operator. Let  $\mathbf{g}$  and  $\mathbf{G}$  be the vectors of  $g(\mathbf{k})$  and  $G(\mathbf{x})$ , respectively. Using this notation, we can rewrite the sum in Eq. (6) as follows:

$$\begin{aligned} \sum_B |G(\mathbf{x})|^2 &= (\mathbf{G}, \mathbf{G})_B = (\mathbf{T}^{-1}\mathbf{g}, \mathbf{T}^{-1}\mathbf{g})_B \\ &= (\mathbf{I}_B \mathbf{T}^{-1} \mathbf{I}_A \mathbf{g}, \mathbf{I}_B \mathbf{T}^{-1} \mathbf{I}_A \mathbf{g})_{N^d} \\ &= (\mathbf{g}, \mathbf{I}_A \mathbf{T} \mathbf{I}_B \mathbf{T}^{-1} \mathbf{I}_A \mathbf{g})_{N^d}. \end{aligned} \quad (8)$$

In the above formulas,  $\mathbf{I}_A \mathbf{T}$  is a  $a \times N^d$  matrix consisting of  $a$  rows of the matrix  $\mathbf{T}$  that correspond with elements in the region  $A$ , the matrix  $\mathbf{I}_B \mathbf{T}^{-1}$  is similarly defined as the  $b$  rows of the matrix  $\mathbf{T}^{-1}$  that correspond with elements in the ROI  $B$ , and the vector  $\mathbf{I}_A \mathbf{g}$  is defined as the

component of the vector  $\mathbf{g}$  which correspond to  $A$ . Let us define the PSWF operator as

$$\mathbf{K}_{A,B} = \mathbf{I}_A \mathbf{T} \mathbf{I}_B \mathbf{T}^{-1} \mathbf{I}_A, \quad (9)$$

$\mathbf{K}_{A,B}$  is an  $a \times a$  matrix with elements

$$\mathbf{K}_{A,B}(\mathbf{k}', \mathbf{k}) = \frac{1}{N^d} \sum_{\mathbf{x} \in B} \exp\{-2\pi i(\mathbf{x}, \mathbf{k} - \mathbf{k}')/N\}. \quad (10)$$

Written in matrix form, the problem becomes solving the equation

$$\lambda = \max\{\mathbf{g}^+ \mathbf{K}_{A,B} \mathbf{g}\}, \quad (11)$$

where '+' represents a transpose operation of a matrix. It is well known that the solution to this problem is the largest eigenfunction of the matrix  $\mathbf{K}_{A,B}$ . Since for all possible situations in MRI,  $b \ll a$  will hold, it is favorable to express  $\mathbf{K}_{A,B}$  in image-space in order to reduce the matrix size. The PSWF operator can be expressed in image-space as a  $b \times b$  matrix by simple manipulation of Eq. (11),

$$\lambda \mathbf{g} = \mathbf{K}_{A,B} \mathbf{g} = \mathbf{I}_A \mathbf{T} \mathbf{I}_B \mathbf{T}^{-1} \mathbf{I}_A \mathbf{g}. \quad (12)$$

Applying  $\mathbf{I}_B \mathbf{T}^{-1}$  to both sides of the equation we obtain

$$\lambda \mathbf{I}_B \mathbf{T}^{-1} \mathbf{I}_A \mathbf{g} = \mathbf{I}_B \mathbf{T}^{-1} \mathbf{I}_A \mathbf{T} \mathbf{I}_B \mathbf{T}^{-1} \mathbf{I}_A \mathbf{g}. \quad (13)$$

Let

$$\boldsymbol{\psi} = \mathbf{I}_B \mathbf{T}^{-1} \mathbf{I}_A \mathbf{g} \quad (14)$$

and

$$\mathbf{K}_{B,A} = \mathbf{I}_B \mathbf{T}^{-1} \mathbf{I}_A \mathbf{T} \mathbf{I}_B, \quad (15)$$

then Eq. (13) becomes

$$\lambda \boldsymbol{\psi} = \mathbf{K}_{B,A} \boldsymbol{\psi}. \quad (16)$$

The operator  $\mathbf{K}_{B,A}$ , the PSWF operator expressed in image-space, is a  $b \times b$  matrix with elements

$$\mathbf{K}_{B,A}(\mathbf{x}', \mathbf{x}) = \frac{1}{N^d} \sum_{\mathbf{k} \in A} \exp\{2\pi i(\mathbf{x} - \mathbf{x}', \mathbf{k})/N\}, \quad (17)$$

where the image-space coordinates  $\mathbf{x}, \mathbf{x}' \in B$ .

Because  $\mathbf{K}_{B,A}$  is a positive-definite matrix, the eigenvalues,  $\lambda_j$ ,  $j \geq 1$  of this matrix are all non-negative. In fact, we have:

$$1 \geq \lambda_1 \geq \lambda_2 \geq \dots \geq \lambda_b > 0. \quad (18)$$

If  $\boldsymbol{\psi}_j = \mathbf{I}_B \boldsymbol{\psi}_j$  are the orthonormal eigenvectors of  $\mathbf{K}_{B,A}$ , then  $\mathbf{I}_A \mathbf{T} \boldsymbol{\psi}_j$  are the orthogonal eigenvectors of  $\mathbf{K}_{A,B}$ . Since

$$\|\mathbf{I}_A \mathbf{T} \boldsymbol{\psi}_j\|^2 = (\boldsymbol{\psi}_j, \mathbf{K}_{B,A} \boldsymbol{\psi}_j) = \lambda_j, \quad (19)$$

we have that

$$\mathbf{g}_j = \mathbf{I}_A \mathbf{T} \boldsymbol{\psi}_j / \sqrt{\lambda_j}. \quad (20)$$

Also

$$\mathbf{G}_j = \mathbf{T}^{-1} \mathbf{g}_j = \mathbf{T}^{-1} \mathbf{I}_A \mathbf{T} \boldsymbol{\psi}_j / \sqrt{\lambda_j}, \quad (21)$$

which gives us

$$\mathbf{I}_B \mathbf{G}_j = \sqrt{\lambda_j} \psi_j. \quad (22)$$

The eigenvalue  $\lambda_j$  is equal to the fraction of the total signal intensity in  $B$  calculated according to Eq. (1) using the corresponding eigenfunction  $\psi_j$ . This maximum fraction of the total signal in  $B$  is equal to  $\lambda_1$ . Hence, the largest eigenfunction  $\psi_1$  is the sought-after function.

Once  $g(\mathbf{k})$  is obtained, the total signal over the ROI  $B$  can be calculated using Eq. (3):

$$\int_B F(\mathbf{x}) \, d\mathbf{x} \propto \sum_{\mathbf{k} \in A} f(\mathbf{k}) g^*(\mathbf{k}). \quad (23)$$

This formula can be justified further with the aid of the prolate spheroidal eigenfunctions. Since the eigenfunctions of  $\mathbf{K}_{B,A}$  form an orthonormal and complete base, we can write the integral of  $F(\mathbf{x})$  over  $B$  as,

$$\int_B F(\mathbf{x}) \, d\mathbf{x} = \sum_j \int_B F(\mathbf{x}) \psi_j \, d\mathbf{x} \int_B \psi_j \, d\mathbf{x}. \quad (24)$$

In the above equation, all the terms for  $j \geq 2$  are small in comparison to the first term and can be ignored [17]. The reason is that the eigenfunctions  $\psi_j$  ( $j \geq 2$ ) oscillate about zero in  $B$ , causing the integral of  $\psi_j$  over  $B$  to be insignificantly small. Thus,

$$\begin{aligned} \int_B F(\mathbf{x}) \, d\mathbf{x} &\approx \int_B F(\mathbf{x}) \psi_1 \, d\mathbf{x} \int_B \psi_1 \, d\mathbf{x} \\ &= \int_B F(\mathbf{x}) G_1(\mathbf{x}) \, d\mathbf{x} \int_B G_1(\mathbf{x}) \, d\mathbf{x} / \lambda_1. \end{aligned} \quad (25a)$$

Since  $G_1(\mathbf{x})$  is essentially zero outside of  $B$  for  $\lambda \approx 1$ , and  $g_1(\mathbf{x})$  is zero outside of  $A$ , we have

$$\begin{aligned} \int_B F(\mathbf{x}) \, d\mathbf{x} &\approx \int_{N^2} F(\mathbf{x}) G_1(\mathbf{x}) \, d\mathbf{x} \int_B G_1(\mathbf{x}) \, d\mathbf{x} / \lambda_1 \\ &= \int_A f(\mathbf{k}) g_1(\mathbf{k}) \, d\mathbf{k} \int_B G_1(\mathbf{x}) \, d\mathbf{x} / \lambda_1. \end{aligned} \quad (25b)$$

Thus, the total signal over  $B$  can be approximately evaluated using Eq. (23).

The largest eigenvalue,  $\lambda_1$ , increases and eventually approaches one as the sampling area of  $k$ -space increases. From Eqs. (1) and (5), (6), the physical meaning of eigenvalue  $\lambda$  is the fractional signal of  $B$  calculated from the reduced  $k$ -space area  $A$  with the PSWF filter. The signal leakage of the filter can be estimated simply by  $1 - \lambda$ . Thus, the eigenvalue  $\lambda$  is a quantitative measure of the corresponding filter performance.

In choosing the number of sampling points,  $a$ , the condition  $\lambda_2 \ll \lambda_1 \cong 1$  should be satisfied. For the two-dimensional case ( $d = 2$ ), the results from a computer search have indicated that this requirement leads to a simple relationship:

$$a = 3N^2/b, \quad (26)$$

where  $b$  is the size of the ROI  $B$  and  $N^2$  is the size of the image. This relationship offers a practical lower limit for choosing  $a$ .

In summary, for a given ROI  $B$  in image-space, the reduced sampling area  $A$  in  $k$ -space is determined first with the approach described above. The PSWF operator corresponding to  $A$  and  $B$ ,  $\mathbf{K}_{A,B}$ , can then be constructed. Subsequently, a 2D filter over  $A$  is obtained by calculating the largest eigenfunction,  $g_1(\mathbf{k})$ , of  $\mathbf{K}_{A,B}$ . The performance of the filter in calculating the total intensity in  $B$ , depends on the size and shape of  $B$ . The best results of this method are obtained if  $B$  is convex. For non-convex  $B$ ,  $g_1(\mathbf{k})$  may lead to significant signal leakage. This problem and its solutions are discussed with demonstrations in Section 4.

### 3. Methods

The 2D-PSWF method was implemented in IDL (Research systems, Boulder, CO 80301, USA) on an AIX workstation. The experimental MRI data were acquired on a MEDSPEC S300 3.0 T research whole body imager (Bruker Instruments, Karlsruhe, Germany) with a quadrature head coil. For fMRI studies, three healthy volunteers (aged 25–35 years, two male and one female) participated in the study with consent from each subject and approval by the institutional review board. The  $T_2^*$ -weighted images from six oblique axial slices along the calcarine sulcus were acquired using an echo planar imaging (EPI) sequence with TR 1000 ms, TE 40 ms, flip angle  $90^\circ$ , field of view  $250 \times 250 \text{ mm}^2$ , slice thickness 5 mm, matrix  $64 \times 64$ , and acquisition bandwidth 143 kHz, while the left lens of a pair of custom-made goggles flashing at 7.8 Hz were turned on for 5 s for visual stimulation (five images) and off for 35 s for baseline (35 images). Each visual stimulation run was repeated four times with an acquisition of 160 images from each slice. The switching of the goggles was controlled by a Grass S10VS Miniature Visual Stimulator (Astro-Med, West Warwick, RI, USA). The fMRI activation map was obtained with the *Stimulate* software [25] by correlating the time-course signal intensity with the stimulation paradigm.

To validate our method experimentally, ROI  $B$  was selected as a circular region containing 21 pixels in the visual cortex from the fMRI activation map. In this case, the heuristic shape of reduced  $k$ -space area  $A$  was also circular with 673 points. The temporal changes of the total signal from  $B$  were calculated using 2D-PSWF and conventional full  $k$ -space methods. To compare the two methods without any possible interference of experimental variations during acquisitions, the same full  $k$ -space data were used for the 2D-PSWF method by discarding the data points outside area  $A$ . The 2D-PSWF for  $A$  was then obtained with  $\lambda_1 = 0.968$ .



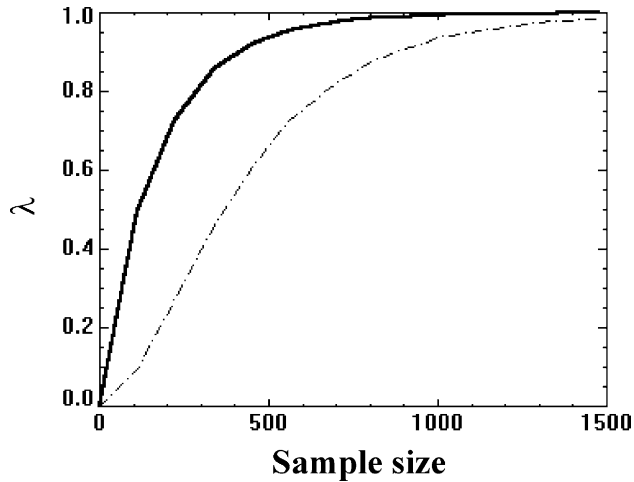


Fig. 3. The first (bold) and second (dashed) eigenvalues plotted as a function of the sample size  $a$  of given ROI  $B$  in Fig. 1.

advisable, as it will lead to signal loss due to a stronger truncation effect.

Our theoretical description of the PSWF method has been presented mostly in  $k$ -space. However, it is more straightforward to visualize the impact of sampling size  $a$  on the total signal intensity from  $B$  by the eigenfunction plots expressed in the image-space. Fig. 4a shows the plots of the 1st eigenfunction in image-space with three different sampling sizes, approximately 1/10, 1/20, and 1/40 of the total number of points of the original image (16,384 points). For  $a = 1635$ , the eigenvalue is up to 0.9996 and the signal distribution is highly focused, indicating that the leakage of energy from  $B$  is insignificant with 1/10th of the original sampling size. This would lead to a significant reduction of the data

acquisition time. With sampling size  $a = 417$ , smaller than the lower bound found with Eq. (26), the eigenvalue reduces to 0.914. Under such conditions the signal intensity distribution starts to show the truncation effect with an obviously broadened center peak and ripples in an extended area. Thus, the sampling area with size  $a = 1635$  is used for the subsequent steps in the simulated fMRI experiment.

#### 4.3. Eigenvalues and eigenfunctions

After determination of  $A$  for the given  $B$ ,  $\mathbf{K}_{B,A}$  is constructed using Eq. (16) and its eigenvalues and eigenfunctions can be obtained. Fig. 4b shows three eigenfunctions corresponding to  $\lambda_1, \lambda_3$ , and  $\lambda_5$  with size  $a = 931$ . The 1st eigenfunction is compact in  $B$ , rendering the largest energy concentration fraction (0.993) in  $B$ , while the 3rd and 5th eigenfunctions are spread out to more extended areas, resulting in a decrease in the corresponding eigenvalue. As indicated in Eq. (18), higher eigenfunctions lead to even smaller eigenvalues. Thus, the 1st eigenfunction is the most suitable choice for  $g(\mathbf{k})$ .

#### 4.4. Calculation of the signal intensity in $B$ with $g(\mathbf{k})$

Once  $g(\mathbf{k})$  is obtained, the total signal intensity from  $B$  can be evaluated directly from the reduced  $k$ -space area using Eq. (3). The time-course signal intensity plots that simulate a fMRI paradigm are shown in Fig. 5. To validate our theory, the total signal intensity from full  $k$ -space is also calculated by direct integration over  $B$  in the phantom images and plotted in dotted lines in Fig. 5. It can be seen in Fig. 5a that with a 10-fold reduction in

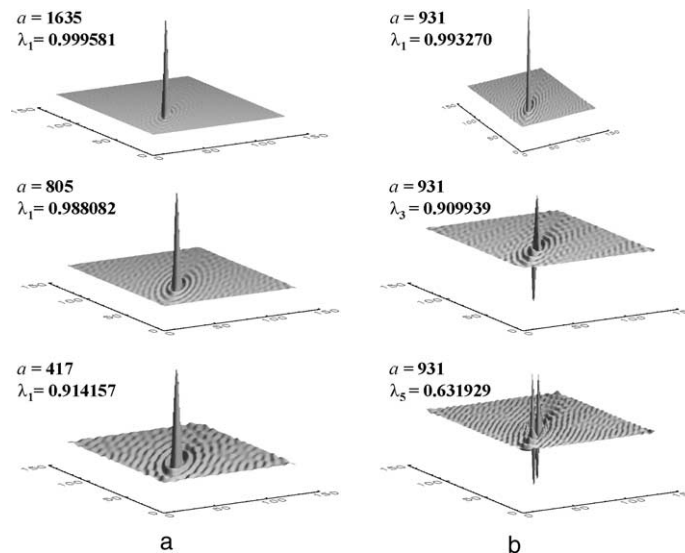


Fig. 4. (a) The plots of the first eigenfunction vs. size  $a$  of  $A$ . (b) The plots of the first, third, and fifth eigenfunctions with  $a = 931$ . All eigenfunction plots are expressed in image-space for a straightforward visualization of the characteristics of PSWFs.

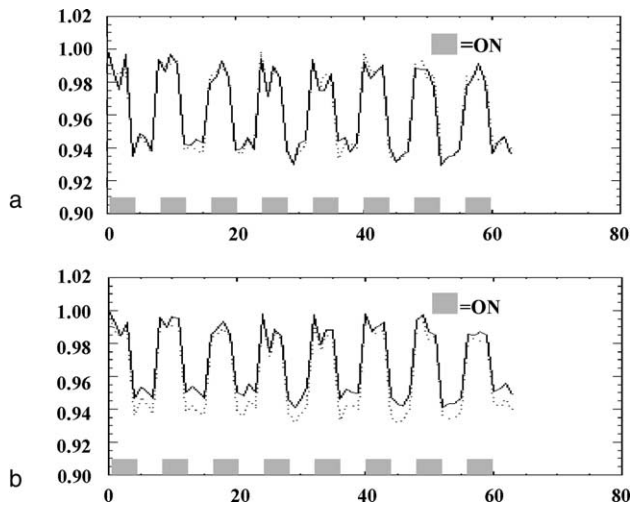


Fig. 5. The time-course signal intensities over  $B$  using the 2D-PSWF method (a) and the keyhole method with same number of points (b). The signal intensity with full  $k$ -space sampling is plotted in dotted lines for comparison. The signal intensity difference between on and off periods is essentially the same for the 2D-PSWF method and is reduced by 20% for the keyhole method.

sampling of  $k$ -space area, the differences in signal intensity, and its temporal variation between the 2D-PSWF and full  $k$ -space methods, are well within the standard deviation of the noise. For comparison purposes, a corresponding signal intensity plot using the keyhole method is shown in Fig. 5b. The sampling regions are kept the same for both 2D-PSWF and keyhole methods. The activation contrast using the keyhole method, however, is reduced by 20%. Thus, the reduction in  $k$ -space sampling area with 2D-PSWF method can substantially increase the temporal resolution without significant SNR penalty.

#### 4.5. Application to experimental data

To validate the theoretical analysis and computer modeling results, the utility of the 2D-PSWF was tested experimentally with fMRI using visual stimulation. Fig. 6 shows time-course plots from an activated region in the visual cortex of a circular shape containing 21 pixels. The solid line in the plot is obtained using the 2D-PSWF method from a reduced  $k$ -space with a circular shape consisting of 673 points with corresponding  $\lambda_1 = 0.968$ . The dotted line in the plot is the signal intensity from  $B$  using full  $k$ -space ( $128 \times 128$ ) time-course data. With about 1/8 of the full  $k$ -space data, the temporal signal intensity changes are very well preserved by the 2D-PSWF method. The Z-scores are 3.46 for full  $k$ -space and 3.88 for reduced  $k$ -space with the 2D-PSWF method. Thus, with our method, such a reduction of  $k$ -space sampling produces no significant change in the detection of the fMRI signal. The reduction of  $k$ -space sampling area can be used to increase the temporal

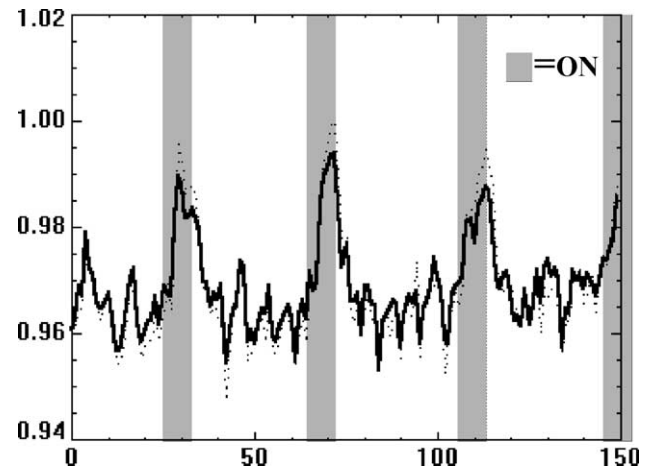


Fig. 6. The time-course signal intensities over an activated ROI in visual cortex consisting of 21 points using the full  $k$ -space (dotted line) and the 2D-PSWF method with 1/8 of the  $k$ -space area (solid line).

resolution for a known activated area. The temporal behavior of the activation signals is important for studying brain function and the associated hemodynamics with MRI. This method is an efficient way to tradeoff spatial resolution within a given ROI for temporal resolution.

## 5. Discussion

Due to hardware limitations, the sampling of  $k$ -space must be economized for dynamic MRI studies. In our method, the reduction of  $k$ -space sampling is realized by trading off spatial resolution. However, unlike the keyhole technique, a reference image is utilized a priori to determine the feature of a ROI. As seen in Fig. 1, the spatial frequency distribution of an asymmetric ROI is anisotropic in  $k$ -space. The isotropic reduction of the sampling of high spatial frequency regions sacrifices the SNR from a given ROI. Tailoring the sampling region and matching the 2D-PSWF filter to the shape and size of a given ROI, allows us to optimize the reduction in  $k$ -space sampling with minimal SNR penalty. The non-square shaped ROI reduces the signal leakage outside the ROI, which also improves the contrast-to-noise ratio (CNR). Partial volume effect is a serious problem in chemical shift imaging. Thus, this method has promising applications in chemical shift imaging to reduce the spectral contamination due to the partial volume and truncation effects.

From a practical point of view, a reliable estimate of the size and shape of the ROI  $B$  is important because the rest of the mathematical treatment on which it is based. A reference image with high spatial resolution can be used to determine ROI  $B$  prior to the dynamic experiment. In choosing the size of the ROI, tradeoffs must be

made among SNR, the reduction of  $k$ -space sampling, and partial volume effects. In practice, shapes of ROI are often curved in 3D rather than in 2D. This method will be eventually extended to 3D, in which case its advantages become more significant.

A 2D-PSWF filter calculated for a specific  $B$  can be used for all its translationally shifted ROIs in the image-space. An alternative ROI,  $B$ , can be obtained by shifting  $B(\mathbf{x})$  to  $B(\mathbf{x} + \mathbf{s})$  in image-space, where  $\mathbf{s}$  is a displacement vector. The corresponding filter,  $G'$ , for this new region can be calculated by taking

$$G'(\mathbf{x}) = \sum_{\mathbf{k} \in A} e^{i(\mathbf{s}-\mathbf{x}) \cdot \mathbf{k}} g(\mathbf{k}), \quad (27)$$

which is equivalent to the well-known shift theorem in Fourier analysis. Thus,  $A$  and the associated  $g(\mathbf{k})$  can be used for calculation of any ROI with the same shape and size. Therefore, having prior knowledge of the exact location of the ROI is of less importance, as one can just shift the ROI slightly if needed during post-processing.

The 2D-PSWF can be applied to conventionally acquired  $k$ -space data as a low-pass filter for post-processing. However, there is an essential difference between the 2D-PSWF and a conventional low-pass filter. The 2D-PSWF filter can be tailored to match the anisotropy of the spatial frequency distribution of an image feature, and thus provides more versatility and efficiency in filtering. As we have demonstrated in Fig. 5, application of the 2D-PSWF filter enhanced the CNR of the fMRI data from the ROI.

In the above discussions,  $B$  is assumed to be convex. For a non-convex ROI, the 2D-PSWF method can be applied by either splitting the ROI into numerous smaller convex ROIs, or in some cases by using a larger convex shape and subtracting the parts that are not included in the ROI. To illustrate the latter case, consider a non-convex ROI of Shape  $S_1$  as shown in Fig. 7. Shape  $S_1$  can be obtained by subtracting the Shape  $S_3$  from Shape  $S_2$ . Since the two ROIs are convex, the total signal intensities from Shape  $S_2$  and  $S_3$ ,  $I_{S_2}$ , and  $I_{S_3}$ , can be calculated separately using the 2D-PSWF method. Because the calculations in the 2D-PSWF method are

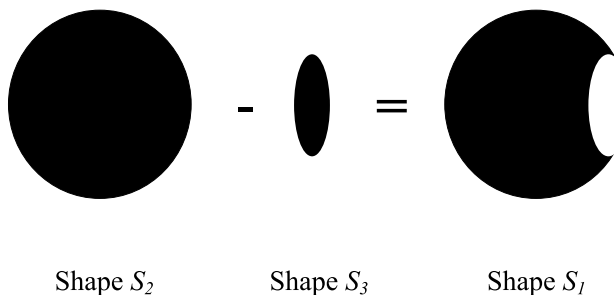


Fig. 7. The 2D-PSWF method can be applied to a non-convex ROI Shape  $S_1$  using linear combination of the two convex regions Shapes  $S_2$  and  $S_3$ .

linear operations, the total signal intensity from Shape  $S_1$  is  $I_{S_1} = I_{S_2} - I_{S_3}$ . Thus, with such an approach, the 2D-PSWF method can be effectively applied to a non-convex case. In this scenario, the sampling area  $A$  is determined by the smaller ROI  $S_3$ .

## 6. Conclusion

The 2D-PSWF method addresses the issues inherent in the fast Fourier transform, such as partial volume effect due to the rectangular voxel shape, and the inverse relationship between image resolution and  $k$ -space sampling area (temporal resolution). These problems are frequently encountered in rapid imaging and chemical shift imaging. This method uses the prior knowledge of a given ROI and the temporal resolution requirement to design a reduced sampling area of  $k$ -space with a matched 2D-PSWF filter such that optimal signal concentration and minimal truncation artifacts are achieved. In this method, the  $k$ -space sampling area is optimally reduced because it matches the anisotropy in resolution posed by the non-rectangular shape of a given ROI. The 2D-PSWF method offers an efficient way for spatial and temporal tradeoff with minimal penalty due to truncation, and thus it promises a wide variety of applications in MRI research.

## Acknowledgment

Special thanks for support from the Whitaker Foundation: RG-99-0157.

## References

- [1] J.J. van Vaals, M.E. Brummer, W.T. Dixon, H.H. Tuithof, H. Engels, R.C. Nelson, B.M. Gerety, J.L. Chezmar, J.A. den Boer, "Keyhole" method for accelerating imaging of contrast agent uptake, *J. Magn. Reson. Imaging* 3 (1993) 671–675.
- [2] J.H. Gao, J. Xiong, S. Lai, E.M. Haacke, M.G. Woldorff, J. Li, P.T. Fox, Improving the temporal resolution of functional MR imaging using keyhole techniques, *Magn. Reson. Med.* 35 (1996) 854–860.
- [3] G.P. Zientara, L.P. Panych, F.A. Jolesz, Dynamically adaptive MRI with encoding by singular value decomposition, *Magn. Reson. Med.* 32 (1994) 268–274.
- [4] L.P. Panych, C. Oesterle, G.P. Zientara, J. Hennig, Implementation of a fast gradient-echo SVD encoding technique for dynamic imaging, *Magn. Reson. Med.* 35 (1996) 554–562.
- [5] L.P. Panych, F.A. Jolesz, A dynamically adaptive imaging algorithm for wavelet-encoded MRI, *Magn. Reson. Med.* 32 (1994) 738–748.
- [6] Z.P. Liang, P.C. Lauterbur, An efficient method for dynamic magnetic resonance imaging, *IEEE Trans. Med. Imaging* 13 (1994) 677–686.
- [7] K.P. Pruessmann, M. Weiger, M.B. Scheidegger, P. Boesiger, SENSE: sensitivity encoding for fast MRI, *Magn. Reson. Med.* 42 (5) (1999) 952–956.

- [8] D.K. Sodickson, W.J. Manning, Simultaneous acquisition of spatial harmonics (SMASH): fast imaging with radiofrequency coil arrays, *Magn. Reson. Med.* 38 (4) (1997) 591–603.
- [9] W.H. Perman, O. el Ghazzawy, M.H. Gado, K.B. Larson, J.S. Perlmutter, A half-fourier gradient echo technique for dynamic MR imaging, *Magn. Reson. Med.* 11 (1993) 357–366.
- [10] S. Ogawa, D.W. Tank, R. Menon, J.M. Ellermann, S.G. Kim, H. Merkle, K. Ugurbil, Intrinsic signal changes accompanying sensory stimulation: functional brain mapping with magnetic resonance imaging, *Proc. Natl. Acad. Sci. USA* 89 (1992) 5951–5955.
- [11] K.K. Kwong, J.W. Belliveau, D.A. Chesler, I.E. Goldberg, R.M. Weisskoff, B.P. Poncelet, D.N. Kennedy, B.E. Hoppel, M.S. Cohen, R. Turner, H.M. Cheng, T.J. Brady, B.R. Rosen, Dynamic magnetic resonance imaging of human brain activity during primary sensory stimulation, *Proc. Natl. Acad. Sci. USA* 89 (1992) 5675–5679.
- [12] T. Ernst, J. Hennig, Observation of a fast response in functional MR, *Magn. Reson. Med.* 32 (1994) 146–149.
- [13] J. Hennig, C. Janz, O. Speck, T. Ernst, Functional spectroscopy of brain activation following a single light pulse: examination of the mechanism of the fast initial response, *Int. J. Imaging Syst. Technol.* 6 (1995) 203–208.
- [14] X. Hu, T.H. Le, K. Ugurbil, Evaluation of the early response in fMRI in individual subjects using short stimulus duration, *Magn. Reson. Med.* 37 (1997) 877–884.
- [15] B. Biswal, F.Z. Yetkin, V.M. Haughton, J.S. Hyde, Functional connectivity in the motor cortex of resting human brain using echo-planar MRI, *Magn. Reson. Med.* 34 (1995) 537–541.
- [16] K. Hendrich, X. Hu, R.S. Menon, H. Merkle, P. Camarata, R. Heros, K. Ugurbil, Spectroscopic imaging of circular voxels with a two-dimensional Fourier-series window technique, *J. Magn. Reson. Series B* 105 (1994) 225–232.
- [17] L. Shepp, C.H. Zhang, Fast functional magnetic resonance imaging via prolate wavelets, *Appl. Comput. Harmonic Anal.* 9 (2000) 99–119.
- [18] Q.X. Yang, L. Shepp, C.H. Zhang, R.J. Demeure, M.B. Smith, A new algorithm of optimal data acquisition and reconstruction for non-square voxel, in: *Proceedings of the 7th ISMRM Annual Meeting, Philadelphia, 1999*, p. 665.
- [19] M. Lindquist, Q.X. Yang, C.H. Zhang, R.J. Demeure, M.B. Smith, L. Shepp, ROI tailored  $k$ -space sampling and a 2D prolate spheroidal wave function filter: reduction of spectral contamination in spectroscopic imaging, in: *Proceedings of the 8th ISMRM Annual Meeting, Denver, 2000*, p. 1842.
- [20] D. Slepian, H.O. Pollak, Prolate spheroidal wave functions, Fourier analysis and uncertainty, I, *Bell System Tech. J.* 40 (1961) 43–64.
- [21] H.J. Landau, H.O. Pollak, Prolate spheroidal wave functions, Fourier analysis and uncertainty, II, *Bell System Tech. J.* 40 (1961) 65–84.
- [22] H.J. Landau, H.O. Pollak, Prolate spheroidal wave functions, Fourier analysis and uncertainty, III, *Bell System Tech. J.* 41 (1962) 1295–1336.
- [23] D.B. Percival, A.T. Walden, *Spectral Analysis for Physical Applications*, Cambridge University Press, Cambridge, UK, 1993.
- [24] D.L. Donoho, P.B. Stark, A note on rearrangements, spectral concentration, and the zero-order prolate spheroidal wavefunction, *Trans. Inform. Theory* 39 (1993) 257–260.
- [25] J.P. Strupp, Stimulate: a GUI based fMRI analysis software package, *NeuroImage* 3 (1996) S607.